GE Nuclear Energy

Sandra A. Delvin
Manager, ESBWR
Engineering & Technology

General Electric Company
175 Curtner Avenue, M/C 307 San Jose, CA 95125-1014
408 925-3900 (phone) 408 925-5490 (facsimile)

Project 717

MFN 03-101
September 19, 2003

Letter 9
Non-Proprietary

U.S. Nuclear Regulatory Commission
Document Control Desk
Washington, D.C. 20852-2738

Attention: Chief, Information Management Branch
Program Management
Policy Development and Analysis Staff

Subject: **Response to Request for Additional Information (RAI) numbers (54, 79, 100, 101, 109, 259, 282, 309, 311, 333, and 383) for ESBWR Pre-application Review.**

GE Nuclear Energy is submitting, in enclosures 1 responses to Requests for Additional Information (RAI) numbers 54, 79, 100, 101, 109, 259, 282, 309, 311, 333, and 383, which were included in the referenced letters. The enclosure contains no proprietary information.

If you have any questions about the information provided here, please let me know.

Sincerely,

Sandra A. Delvin
Manager, ESBWR
Engineering & Technology

D068

Reference:

1. MFN 03-052, Letter From Amy E. Cubbage (NRC) To Atam S. Rao (GE), June 20, 2003, SUBJECT: REQUEST FOR ADDITIONAL INFORMATION LETTER NO. 4 RELATED TO ESBWR PRE-APPLICATION REVIEW (TAC NOS. MB6283 AND MB6801)
2. MFN 03-053, Letter From Amy E. Cubbage (NRC) To Atam S. Rao (GE), July 17, 2003, SUBJECT: REQUEST FOR ADDITIONAL INFORMATION LETTER NO. 5 RELATED TO ESBWR PRE-APPLICATION REVIEW (TAC NOS. MB6279, MB6281, AND MB7255)
3. MFN 03-054, Letter From Amy E. Cubbage (NRC) To Atam S. Rao (GE), July 17, 2003, SUBJECT: REQUEST FOR ADDITIONAL INFORMATION LETTER NO. 6 RELATED TO ESBWR PRE-APPLICATION REVIEW (TAC NO. MB6801)
4. MFN 03-065, Letter From Amy E. Cubbage (NRC) To Atam S. Rao (GE), July 17, 2003, SUBJECT: REQUEST FOR ADDITIONAL INFORMATION LETTER NO. 7 RELATED TO ESBWR PRE-APPLICATION REVIEW (TAC NO. MB6801)
5. MFN 03-066, Letter From Amy E. Cubbage (NRC) To Atam S. Rao (GE), July 17, 2003, SUBJECT: REQUEST FOR ADDITIONAL INFORMATION LETTER NO. 8 RELATED TO ESBWR PRE-APPLICATION REVIEW (TAC NOS. MB6280 AND MB6281)

Enclosures:

1. MFN 03-082 Responses to RAI numbers (54, 79, 100, 101, 109, 259, 282, 309, 311, 333, and 383) - Non-proprietary Information

cc:	A. Cubbage	USNRC (with enclosure)
	J. Lyons	USNRC (w/o enclosure)
	G.B. Stramback	GE (with enclosure)

ENCLOSURE 1

MFN 03-101

Response to NRC RAI numbers (54, 79, 100, 101, 109, 259, 282, 309, 311, 333, 383)

Q54. Section 6.5.3.2 - Bubble number density has a minimum (lower) limit of 10^7. Bubble size also has an upper and a lower limit. What is the basis of these limits? Are these limits (large bubble size and void fraction for bubbly flow) mutually consistent for bubbly flow? Similar limits were found for droplet flows in Section 6.5.5.

R54. The limits on the bubble sizes for the calculation of the interfacial heat transfer are chosen to keep the bubble size and the interfacial heat transfer within reasonable bounds. The upper boundary is given by the geometry. Theoretically the maximum bubble size would be given by the hydraulic diameter, however due to the fact that the spacers will break up the bubbles in a fuel channel an upper limit of half the hydraulic diameter was chosen. For a fuel channel, which has the smallest hydraulic diameter of the BWR components, this would lead to an upper limit of [[ ]]. The lower limit of 0.0005 m was chosen to prevent the interfacial heat transfer from becoming too large, which can lead to numerical difficulties. For very large interfacial heat transfer rate, the phases will be in thermal equilibrium and the results are not very sensitive to the exact value of the interfacial heat transfer. For typical operating conditions, the bubble sizes will be in the range of [[ ]], and the number density will be in the range of [[ ]], and are therefore not affected by the limits. Similar arguments are applied for droplet flow, in order to keep the interfacial heat transfer within reasonable bounds. The good comparison to the void fraction and heat transfer data shows that these limits do not adversely affect the results.

Q79. Section 7.5.2.7 (p. 7.5-18) - Is there any documented comparison between the gap conductance calculated by TRACG and other referenced GE models and codes?

R79. The fuel gap conductance models in Sections 7.5.2 and 7.5.3 are identical to the SAFER/GESTR models approved by the NRC, and also reviewed in the TRACG application for AOOs.

The TRACG implementation was verified against SAFER as part of the TRACG testing. An example of this testing is shown in Figure 79-1. The comparison was done for a small break LOCA case. The initial values agreed perfectly and small differences developed during the transient due to differences in the hydraulic model.

[[

]]

Q100. Section 3.4.1.2 (p. 3-48) - What was the uncertainty of the pressure measurement?

R100 The uncertainty in the pressure measurement for the Marviken critical flow tests is 90 kPa [Reference 100.1].

Reference 100.1: TRACC-M/F77, Version 5.5 Developmental Assessment Manual, NUREG/CR-6730, Vol.1, page 4.3-2, July 2001.

Q101. Section 3.4.1.5 (p. 3-48) - Why did TRACG predict much higher break flow rate than the data for the initial 5 seconds for both Tests 15 and 24?

R101. Due to the high sonic velocity in subcooled liquid the break flow is expected to increase to its maximum value almost instantaneously. The transit time for a sonic wave in the subcooled liquid in the nozzle and discharge pipe is approximately 5 msec. This behavior is calculated by TRACG. The delay in the measured break flow as seen most clearly in test 24 is most likely due to lag in the instrumentation.

The TRACG comparison to the measured break flow for Marviken test 24 is shown in Figure 101-1. The measured break flow is based on a measurement of the liquid inventory in the vessel. The measurement uncertainty for this measurement is 15-20% (TRAC-M Development Assessment Manual, NUREG/CR-6730). There was also a Pitot tube measurement of the flow. This measurement is most reliable for single-phase conditions. Both measurements are shown in Figure 4.3-16 from NUREG/CR-6730. This Figure is shown below in Figure 101-2. It is seen that the flow measurement from the Pitot tube is in very close agreement with the calculated flow in the initial 5 seconds of the test.

[[

]]

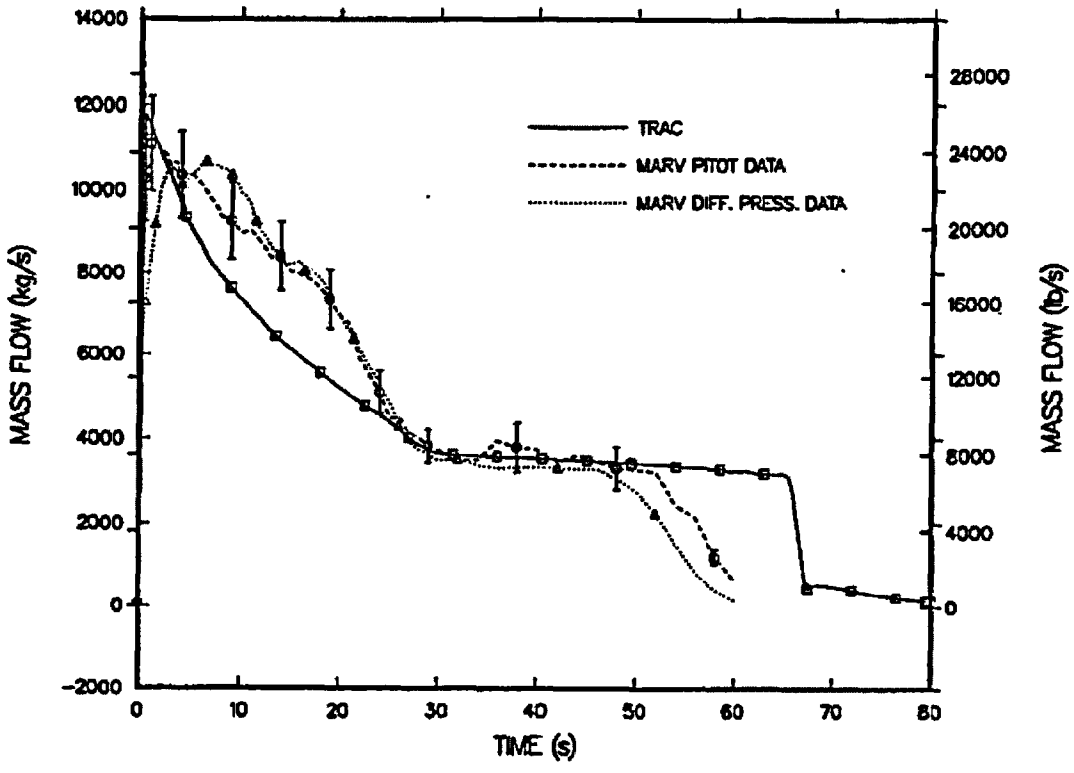

Fig. 4.3-16. Break-flow comparison for Marviken Test 24.

Figure 101-2. NUREG/CR-6730 Figure 4.3-16

Q109. Section 5.1.1.3 (p. 5-4) - How is the uncertainty in the measured nodal void fraction related to the smoothing of the data?

R109. The measured pressure drop showed fluctuations which were removed in the smoothed data. The smoothed data were then converted to a void fraction assuming that the measured pressure drop is entirely due to the static head. The magnitude of the fluctuations in the pressure drop plus the uncertainty in the pressure drop measurement when converted to an equivalent static head corresponds to a 5% uncertainty in average void fraction between the pressure tab locations.

Q259. In the formulation of the generic governing equation, two elements require additional documentation:

Q259.1 The explicit representation of the condensation processes in the PCCS is the key element that links the system to its ultimate heat sink (the PCCS pool). How can the pressure be determined in the intermediate and long-term portion of the transient without the inclusion of this element?

R259.1 It is true that the PCC links the containment to its ultimate heat sink. The manner in which the PCC heat removal capacity relates to the pressure is indirect, however, by influencing the suppression pool surface temperature. [[

]]

The containment pressure in the intermediate and long term portions of a LOCA is set by the wetwell pressure. The wetwell pressure is equal to the sum of the noncondensible partial pressure and the steam partial pressure. The steam partial pressure is equal to, or very close to, the saturation pressure corresponding to the suppression pool surface temperature for most periods of a LOCA. Therefore the containment pressure is influenced by the surface temperature of the suppression pool.

The dominant cause of the increase in containment pressure is the movement of Nitrogen from the drywell to the wetwell during the initial (blowdown) portion of the transient. The majority of the noncondensible gas moves to the wetwell during the early portion of a transient as a result of blowdown forcing a mixture of steam and noncondensible gas through the main vents and PCC vents. There is a secondary contribution to the pressure increase caused by the increase in suppression pool surface temperature resulting from condensation of steam in the suppression pool during blowdown. A much smaller quantity of noncondensibles move through the PCC vent to the wetwell during later periods of the transient as a result of the PCC vent clearing noncondensibles from the PCC.

The effect of the PCC is to minimize the quantity of uncondensed steam that enters the suppression pool and thereby minimize the increase in the steam partial pressure in the wetwell gas space. During blowdown, the PCC reduces the quantity of steam that passes through the main vent to the suppression pool. For the intermediate and long-term portions of a transient the PCC has excess heat removal capacity (i.e. it can remove more energy than the load resulting from decay heat). During these periods the PCC self-regulates to the decay heat load by partially filling with noncondensible gas. The effect of differing PCC heat removal capacities is to change the timing when the PCC can accommodate the entire decay heat load and to change the integrated energy that goes into the suppression pool prior to the time when the decay heat load is matched by the PCC capacity.

To appreciate the dominant role of noncondensible transfer for post-LOCA containment pressurization, it is useful to examine the pressurization rate equation as applied to the wetwell during blowdown. The generic nondimensional pressure rate equation is given by equation 6.1-5 of the ESBWR scaling report as,

$$f_2^+ V^+ \frac{dP^+}{dt^+} = \sum_k \Pi_{P,\dot{Q},k} \dot{Q}_k^+ - \Pi_{P,\dot{V}} P^{*+} \frac{dV^+}{dt^+} + \sum_i \Pi_{P,Wh,i} W_i^+ h_i^+ + \frac{P^{*+}}{\rho^+} \sum_i \Pi_{P,mech,i} W_i^+ - V^+ \sum_j \Pi_{P,y,j} \left(f_{1,j}^+ \frac{dy_j^+}{dt^+} \right) \quad (259\text{-}1)$$

where the terms in the equation are defined on pages 6-4 and 6-5 of the report. The processes of interest to the WW are shown in Figure 7-7 of the report. The table below shows the reference parameters for the ESBWR during blowdown. The resulting PI groups are shown in the bar chart below the table. [[

RAIs NEDC-33082P "ESBWR Scaling Report"
Specific Questions

]]

To see how the PCC participates in the containment pressurization transient, we can look at the energy equation for the suppression pool. The generic nondimensional energy equation is given by equation 6.1-3 of the ESBWR scaling report as,

$$M^{+}\frac{de^{+}}{dt^{+}} = -\Pi_{e,\dot{V}}P^{+}\frac{dV^{+}}{dt^{+}} + \sum_{k}\Pi_{e,\dot{Q},k}\dot{Q}_{k}^{+} + \sum_{i}\Pi_{e,Wh,i}W_{i}^{+}h_{i}^{+} + \frac{P^{+}}{\rho^{+}}\sum_{i}\Pi_{e,mech,i}W_{i}^{+} \quad (259\text{-}2)$$

[[

]]

This PI group for the vents is given by,

$$\Pi_{e,Wh,vents} = \frac{W_{vents}\Delta h_r t_r}{M_o \Delta e_r} \tag{259-4}$$

[[

]]

Q259.2 The derivation of the vapor generation equation in Appendix B of NEDC-32288P, "SBWR Scaling Report," is referenced to the book of Lahey & Moody. In consulting the reference, there is no trace of such equation. Please provide a detailed basis for the derivation of this crucial result, including any assumptions.

R259.2 For the derivation of the vapor generation equation see Section 2.4.3 of "Two-Phase Flow in Complex Systems" by Solomon Levy. Equation 2.4.13 of that reference is for the vapor generation rate and the derivation is described. Future revisions of the report will refer to this alternate reference. For convenience, a copy of the relevant pages is in the attached file.

Q282. The elimination of the PCCS pool from the scaling considerations as the ultimate sinks has some significant implications. One clear implication of this approach is the pseudo-resolution of the non-condensible issue. Specifically, consider the statement on page 6-6: _Therefore the change in condensible fraction is set to 5% which will bound the range that would occur after a VB opening moves noncondensibles to the DW and then back to the WW_. The fundamental reason to conduct PANDA testing is indeed to resolve the non-condensible issue after the opening of VBs. The implication of the extent of mixing or segregation bears immediate consequences on the PCCS operation and therefore on the heat removal from the containment. Setting a _bounding_ value appears quite arbitrary. How is this justified?

R282. The importance of the PCC pool (and, more generally, PCCS heat removal capacity) from the standpoint of scaling has been addressed in the response to RAI 259, part 1 by evaluation of the terms in the non-dimensional energy equation for the suppression pool. The purpose of the PANDA tests has been addressed in the response to RAI 291, where it was stated the PANDA facility "provided information on noncondensable release over a wide range of timing and rates". This was done because of the difficulty in predicting the specific noncondensible fraction in the drywell at a given time and covers a range of conditions that will bound those expected in the ESBWR.

The selection of 5% noncondensible fraction is somewhat arbitrary and is used to show how the noncondensible contribution would be scaled for this particular single value. In retrospect, the word "representative" would have been a preferable characterization. It is easy to see that the noncondensible contribution shown in Figure 8-7 ("bubbles" term in the bar chart) would double for twice this fraction and would be ~20% of the value shown if the noncondensible fraction was 1% rather than 5%. The scaling only allows us to show a single value for the noncondensible contribution but there is a range of possible noncondensible fractions depending on the specific case considered. Because of the uncertainty, the tests covered a wide range of noncondensible conditions as discussed above.

Q309. Provide plots similar to Figures 3.7-2 through 3.7-15 in Section 3 of NEDC-33083P for the ECCS/LOCA calculations presented in Section 2 of NEDC-33083P (time frame 0 to 2000 seconds). These plots will provide a means to assess modeling differences, if they exist, between the modeling of containment for core performance versus the modeling of containment for containment performance.

R309. A set of plots from the ECCS/LOCA case for the Main Steam Line break with one GDCS injection valve failure (Table 2.4-2, NEDC-33083P) is attached here as Figures 309-1 to 309-7. This case uses nominal plant conditions and these figures correspond to those for the Containment/LOCA base case (Figures 3.7-2 to 3.7-9).

It should be mentioned that there are several key nodalizational differences between the ECCS/LOCA and the Containment/LOCA cases. These differences contribute to higher DW pressure (about [[ ]]) response for the ECCS/LOCA case for the first few hundred seconds. The longer term response is not impacted.

The ECCS case uses a more detailed nodalization to model the reactor internals (including heat structures and inventory distribution) such as the guide tubes, shroud wall and steam separators. This detailed modeling of the RPV internals provides better simulation of the RPV response, and calculates a slower depressurization rate for the RPV. The MSL break flow is slightly larger because of the higher RPV pressure and results in a higher DW pressure compared to the Containment case. The Containment case uses a simplified RPV nodalization that does not model the reactor internals. This is the main contributor to the difference in the results. Hence, the ECCS case is judged to be more accurate for the early blowdown response and provides a more realistic time of GDCS initiation.

For the containment case, the initial peak DW pressure following the main vent clearing could be under-estimated by a few psi due to lower break flow as a result of the simplified RPV nodalization. However, this simplification has no impact on the containment design because the maximum DW pressure is determined by the long-term peak pressure, which is higher than the initial peak for the limiting main steam line break case.

Additional differences in the nodalization between the two cases are the main vent modeling and PCC pool temperature. The ECCS case uses [[

]] The Containment case models [[
]] which discharges

horizontally into the suppression pool. A constant PCC pool temperature of [[ ]] is assumed for the ECCS case, while the initial PCC pool temperature is [[ ]] for the Containment case. The containment model is more representative of the plant in this case. However, these items contribute to only about 1/3 of the DW pressure differences between the ECCS and Containment models seen in the early phase of the transient.

[[

]]

Q311. Provide a table of the mass flow rate (kg/sec) and energy (J/sec) from the MSLB pipe break into the drywell for the base case (Section 3.7.2 of NEDC-33083P) and the bounding case (Section 3.7.3 of NEDC-33083P). The time between data points should be sufficiently small such that integrating the tabular data would match the integrated values at the time of GDCS injection, and to capture the timing of the suppression pool vents opening and closing and to be useful in performing a CONTAIN audit analysis of the blowdown portion of the accident (data to the onset of GDCS flow is adequate). Also provide the average reactor pressure vessel conditions at the start of GDCS injection - water inventory, steam inventory, average pressure and average temperature, and the times of each trip signal up to GDCS injection.

R311. Tables 311-1 and 311-2 provide the mass flow rate and energy from the MSLB pipe break into the drywell for the base case and bounding case. Figure 311-1 presents break mass flow rate for the two cases. Figure 311-2 presents energy through the break for the two cases.
It should be mentioned that for long-term containment pressure, the SBWR uncertainty analyses (NEDE-32178P Rev.1) showed that a smaller critical flow multiplier results in higher DW peak pressure. Hence, a model parameter of [[ ]] was applied to the critical flow for the bounding case (PIRT84, Table 3.7-1, NDEC-33083P). If the short-term peak pressure were the figure of merit, a multiplier of [[ ]] would have been employed.

Average RPV conditions at or around the start of GDCS injection

MSLB Base case (at 540 seconds)
Average RPV pressure = [[ ]] Pa
Average temperature = [[ ]] K
Water inventory = [[ ]] kg
Steam inventory = [[ ]] kg

Trip signal
Power scram at [[ ]] seconds
MSIV closure initiated at [[ ]] seconds
Level 1 confirmed at [[ ]] seconds

MSLB Bounding case (at 600 seconds)
Average RPV pressure = [[ ]] Pa
Average temperature = [[ ]] K
Water inventory = [[ ]] kg
Steam inventory = [[ ]] kg

Trip signal

Power scram at [[ ]] seconds
MSIV closure initiated at [[ ]] seconds
Level 1 confirmed at [[ ]] seconds

Table 311-1. Base Case Main Steam Line Break Mass Flow Rate and Energy
[[

Time (s)	Break Flowrate (kg/s)	Energy (J/s)

]]

Table 311-2. Bounding Case Main Steam Line Break Mass Flow Rate and Energy
[[

Time (s)	Break Flowrate (kg/s)	Energy (J/s)

]]

[[

]]

Q333. In order to verify the TRACG critical flow model, we have developed and run a simple test problem. It consists of two break components and a pipe component. Two break components define the pressure boundary conditions (73 bar upstream and atmospheric pressure downstream). A pipe with an orifice at the center was initially set to 73 bar through out its entire length. Then, the downstream break is depressurized to atmospheric pressure. The TRACG code predicts choke condition at the orifice. However, the calculated fluid velocity at the choke point is only about 60 meters per second. Usually, the sound speed is expected to have be on the order of 100 - 300 meters per second. Therefore, the calculated choke flow velocity appears to be lower than the sound speed. Please provide a separate effect test benchmark TRACG deck to assist the staff's further review.

R333. The sonic velocity varies as a function of stagnation pressure and quality at the choke plane. Both have a strong effect on the velocity of sound in homogenous, equilibrium mixtures (HEM) of steam and water. These relationships are shown in Figure 6.11 on page 146 of Graham Wallis's book One-dimensional Two-phase Flow (McGraw Hill, New York, 1969). Wallis attributes the figure to H. B. Karplus (1958). For convenience, it is reproduced here as Figure 333-1. The figure shows that one should expect that for a pressure of 73 bar (1059 psia) that the HEM sonic velocity is approximately 50 m/s for qualities of 0.05 or lower. At the choke plane where the pressure is lower, the sonic velocity is even lower.

The sonic velocity is discontinuous at qualities of 0.0 and 1.0 corresponding to the transitions between single-phase and two-phase flow. This discontinuity in sonic velocity is due to the discontinuity in the specific heat at constant volume (C_v) that occurs at these points. The fact that this will lead to a discontinuity in the sonic velocity is evident from equations (D-10), (D-17) and (D-18) in Appendix D of NEDE-32176P (Rev. 2). This discontinuity is the reason that the sonic velocity can be as much as an order of magnitude lower for low-quality steam-water mixtures than it is for single-phase saturated liquid at the same pressure.

Appendix E of NEDE-32176P (Rev. 2) contains the derivation of the HEM sonic velocity that is used in TRACG. The crux of the problem is to define the compressibility at constant entropy. The simplified form with no noncondensible gas is presented in Eq. (E-40). Free and Spore have obtained the same result (see References 6.3-1 and 6.3-2 cited in NEDE-32176P, Rev. 2). The conclusion is that the fluid velocity of approximately 60 m/s calculated by TRACG at the choke point is a reasonable value.

A proof of the adequacy and applicability of the TRACG critical flow model is the qualification against separate effects critical flow experiments that is documented in Section 3.4 of NEDE-32177P, Rev. 2. The Edwards blowdown problem described

in Section 3.4.3 is a good one to consider both because of its simplicity and because it involves critical flow for a wide range of void fractions. Selected calculated results are compared to test data in Figures 3.4-16 and 3.4-17 of NEDE-32177P, Rev. 2. The TRACG input deck for the Edwards blowdown problem is transmitted in the separate ASCII file named "EDWARDS.INP". The corresponding pressure and void fraction data are contained in the ASCII file named "EDWARDS.DAT".

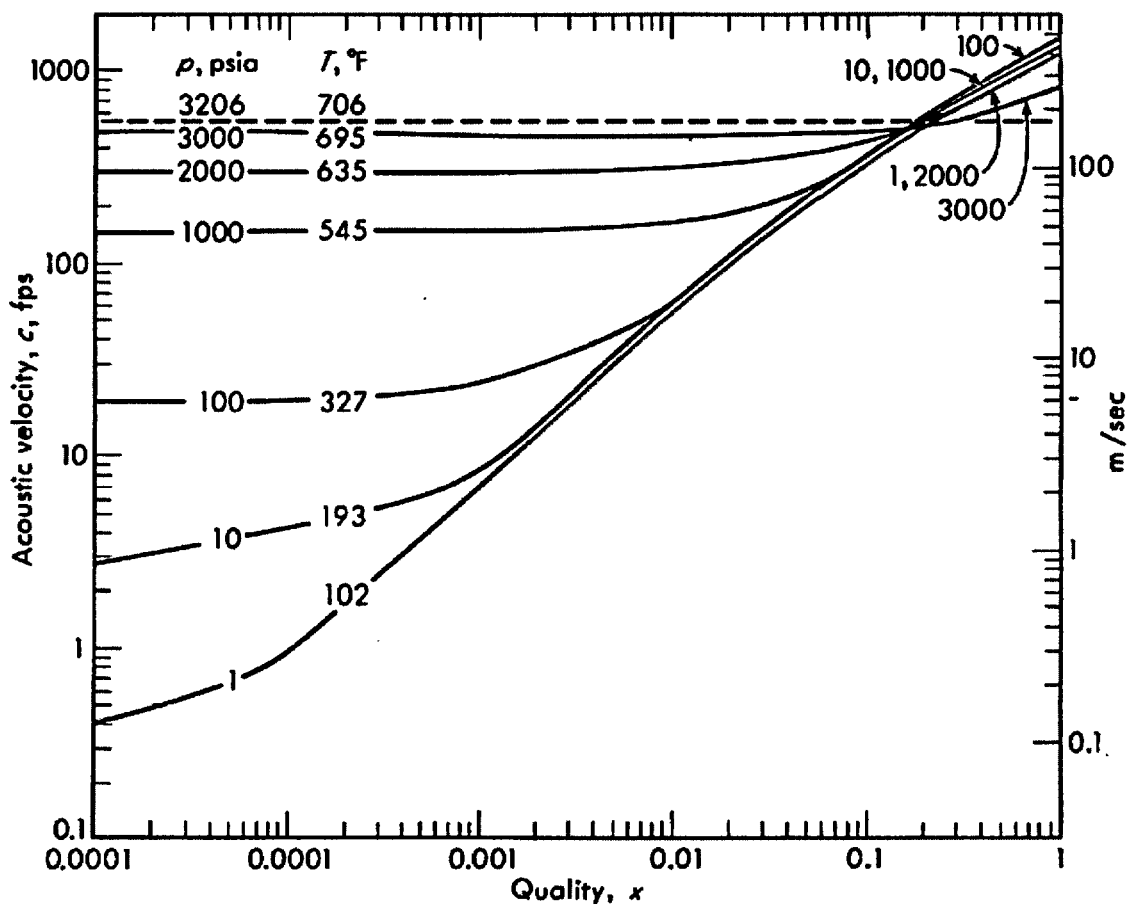

Figure 333-1 Theoretical Sonic Velocity for HEM of Steam and Water

R383. Supplementary Information for RAI383

A figure comparing the DW and WW pressures from GIRAFFE Test T1 and the earlier GIRAFFE test that T1 "tied back" to is attached below. The earlier test, performed in 1992, was designated "Phase 2 MSLB". The initial conditions for these two tests were nominally identical. The two sets of pressures are in good overall agreement. [[

]]